ACSNANO

www.acsnano.org

ARTICLE

Nanoelectronic Investigation Reveals the Electrochemical Basis of Electrical Conductivity in *Shewanella* and *Geobacter*

Mengning Ding,[†,‡,○] Hui-Ying Shiu,[†,‡,○] Shiue-Lin Li,[§] Calvin K. Lee,[‡,∥] Gongming Wang,[‡,∥] Hao Wu,[†] Nathan O. Weiss,[†] Thomas D. Young,[‡,⊥] Paul S. Weiss,[†,‡,⊥] Gerard C. L. Wong,[‡,∥,⊥] Kenneth H. Nealson,[§] Yu Huang,*[,†,‡] and Xiangfeng Duan*[,‡,⊥]

[†]Department of Materials Science and Engineering, [‡]California NanoSystems Institute, [∥]Department of Bioengineering, and [⊥]Department of Chemistry and Biochemistry, University of California, Los Angeles, Los Angeles, California 90095, United States

[§]Department of Earth Sciences and Biological Sciences, University of Southern California, Los Angeles, California 90089, United States

Supporting Information

ABSTRACT: **The electrical conductivity measured in *Shewanella* and *Geobacter* spp. is an intriguing physical property that is the fundamental basis for possible extracellular electron transport (EET) pathways. There is considerable debate regarding the origins of the electrical conductivity reported in these microbial cellular structures, which is essential for deciphering the EET mechanism. Here, we report systematic on-chip nanoelectronic investigations of both *Shewanella* and *Geobacter* spp. under physiological conditions to elucidate the complex basis of electrical conductivity of both individual microbial cells and biofilms. Concurrent electrical and electrochemical measurements of living *Shewanella* at both few-cell and the biofilm levels indicate that the apparent electrical conductivity can be traced to electrochemical-based electron transfer at the cell/electrode interface. We further show that similar results and conclusions apply to the *Geobacter* spp. Taken together, our study offers important insights into previously proposed physical models regarding microbial conductivities as well as EET pathways for *Shewanella* and *Geobacter* spp.**

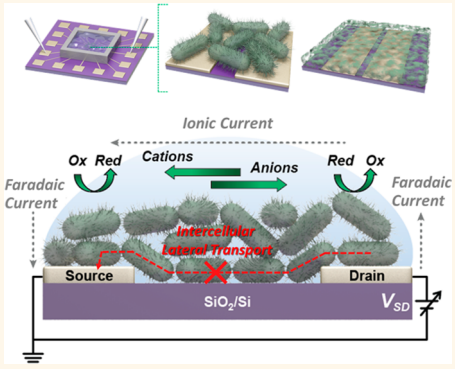

KEYWORDS: *electrogenic bacteria, microbial electrochemistry, bioelectrochemical system, bioelectronics, nanoelectronics, extracellular electron transfer, microbiome*

Dissimilatory metal-reducing bacteria, such as *Shewanella* and *Geobacter* spp., harness energy through the metabolic oxidation of electron donors (organic sources/fuels) and subsequent electron transfer to insoluble electron acceptors (minerals).[1] The electron transfer from *Shewanella* and *Geobacter* spp. to solid-state minerals or electrodes outside the cell, referred to as extracellular electron transport (EET), plays an important role in global biogeochemical cycles[2] and serves as the fundamental working principles for microbial biofuel productions[3−6] and microbial fuel cell (MFC) technologies.[3,7−13] Despite considerable interest, the mechanism for EET remains unresolved, with various possible pathways proposed.[9,14,15] Among them, one hypothesis suggests that long-range electron transport occurs through the electrically conductive biofilm, allowing multiple layers of cells in the biofilm to interact with electrode for respiration. This pathway is based on the unusual electrical conductivity measured in *Shewanella* and *Geobacter* spp., which is intriguing but controversial. To date, studies of the conductive mechanism of *Shewanella* have been inconclusive as most measurements were carried out under *ex situ* nonphysiological conditions.[16,17] For *Geobacter*, electrical measurements have been performed in living biofilms, although the accuracy and interpretation of the data are the subject of ongoing debate.[18−24] Two conflicting models have been suggested to explain the measured electrical conductivity in *Geobacter* nanowires and biofilms. One hypothesis suggests that electron conduction is redox activity (also referred to as multistep electron hopping or a superexchange mechanism), which occurs through electron hopping between adjacent cofactors in the form of a series of redox exchange reactions,

Received: June 2, 2016
Accepted: October 27, 2016
Published: October 27, 2016

DOI: 10.1021/acsnano.6b03655
ACS Nano 2016, 10, 9919−9926

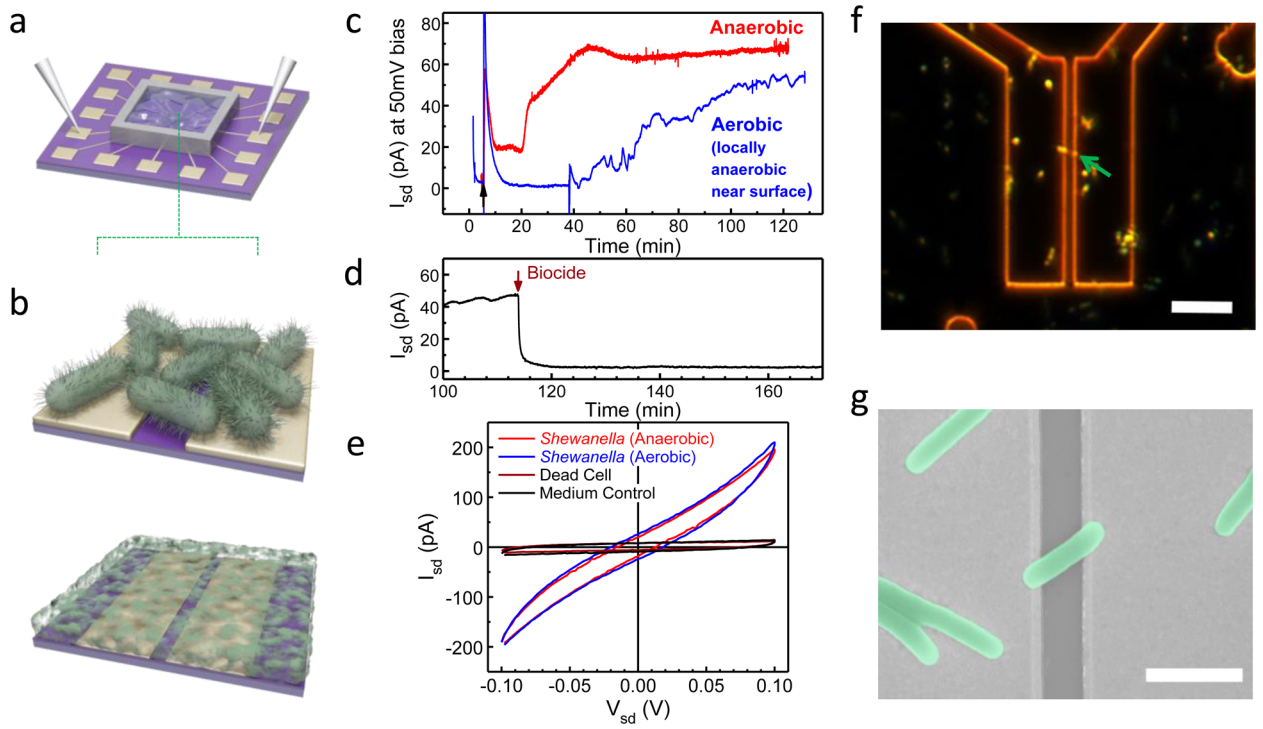

Figure 1. Electrical measurements of *Shewanella oneidensis* MR-1 under physiological conditions. (a, b) Schematic illustration of the nanoelectronic measurement setup with on-chip pair electrodes bridged by either individual MR-1 cells or biofilms. (c) Representative source−drain current (I_{sd}) of living MR-1 as a function of incubation time on the device, under either aerobic or anaerobic conditions. The arrow indicates the injection of MR-1 cells into the measurement chamber. (d) Source−drain current (I_{sd}) of dead MR-1 cells, the arrow indicates the biocide addition. (e) Representative I_{sd}−V_{sd} transport characteristics of individual MR-1 cells, acquired after 2 h on-chip incubation. (f) *In situ* optical microscope (OM) image (dark-field mode) of MR-1 (indicated by green arrows) attached to the electrodes and bridging the gap. (g) *Ex situ* SEM image of MR-1 bridging the gap between pair electrodes (MR-1 cells are false colored for better visualization). Scale bars are 10 and 2 μm in (f) and (g), respectively.

and is often accompanied by a redox gradient (a concentration gradient of oxidized or reduced cofactors).[21,22] Another hypothesis posits an intrinsic metallic-like conductivity of *Geobacter* biofilms. In this model, electron transport occurs through delocalized electronic states along microbial nanowires, nanofilaments made of pilin proteins, with π−π stacking of aligned aromatic moieties in pili.[20] These two contrasting models imply significantly different EET mechanisms and entail distinct compositional and structural architectures of microbial nanowires and extracellular matrix involved in long-range electron transport. Therefore, a comprehensive understanding of the charge transport characteristics is critical for elucidating the functional and structural details and the fundamental conduction mechanism(s) of long-range electron transport in these electrogenic microbial systems.

In order to address this issue and to decipher the origins of the apparent electrical conductivity observed in the *Shewanella* and *Geobacter* systems, we investigated extracellular electron transport in detail at the nanoscale under physiologically relevant conditions. Standard on-chip nanoelectronic testing approaches offer ideal platforms for this purpose. However, the implementations of micro/nanoelectrode arrays to date have focused on measurements of either microbial nanowires under dry (nonphysiological) conditions[16,17] or electrochemical activity of actively respiring microbial systems.[25,26] Interdigitated electrode arrays have been employed for electrical measurements of living *Geobacter* biofilms, but with indirect electrochemical bipotentiostat measurements.[21,22,24] Here, we report systematic on-chip electrical transport studies of *Shewanella oneidensis* MR-1 and *Geobacter sulfurreducens* PCA under physiological conditions using standard nanoelectronic approaches along with concurrent on-chip electrochemical measurements. These more comprehensive measurements elucidate the electrochemical origin of the apparent conductivity in *Shewanella* and *Geobacter*.

RESULTS AND DISCUSSION

Figure 1a,b schematically illustrates the measurement setup and electrode layout used for probing the electrical transport in microbial cells and biofilms. Electrode pairs (source and drain) were prepatterned on a Si/SiO_2 wafer using electron-beam lithography (EBL), and a poly(dimethylsiloxane) (PDMS) chamber was employed to control exposure of electrodes to the microbial samples in the appropriate medium. To obtain better control of the local environment during measurements and to enable independent current recordings from multiple electrodes, an insulating and electrochemically inert polymer layer was employed to define a testing window through a secondary step of EBL. The confined window also enables the precise control of the exact electrode area exposed to the microbial samples, which is an important parameter that has not been thoroughly investigated in previous studies. The gap between the electrode pairs was set to be 1 μm, which is smaller than the typical length of a MR-1 or PCA bacterium. This setup enables measurements of electron transport at the single-cell level, where an individual cell bridges the electrode pairs. We have also used relatively long electrode pairs (up to 3000 μm) to maximize the numbers of bridging cells and thus to amplify the

DOI: 10.1021/acsnano.6b03655
ACS Nano 2016, 10, 9919−9926

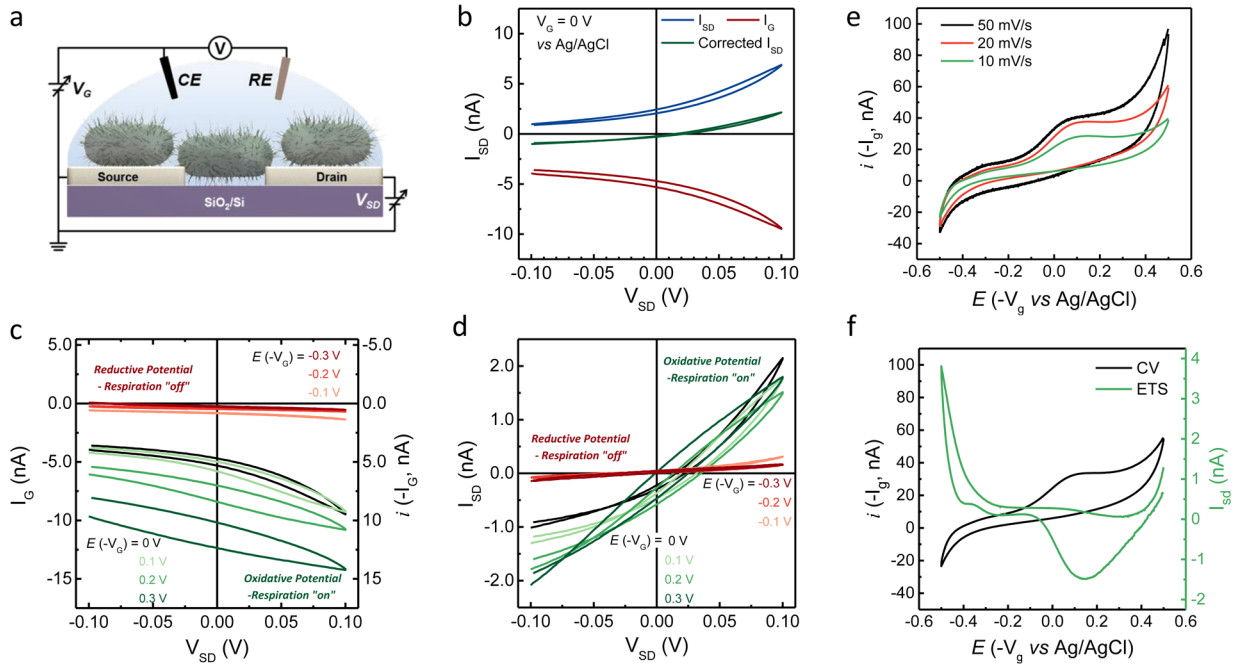

Figure 2. On-chip ETS measurements of *S. oneidensis* MR-1. (a) Schematic illustration of the concurrent measurements of electrochemical (I_g) and electrical transport (I_{sd}) characteristics of MR-1. (b) Representative I_{sd}–V_{sd} (blue) and I_g (red) behavior of living MR-1 cells at 0 V gate voltage (*vs* Ag/AgCl), green curve represents the I_{sd} curve after gate current correction. (c, d) Representative I_g (c) and I_{sd}–V_{sd} (d) curves of living MR-1 at different gate voltages (from −0.3 to 0.3 V *vs* Ag/AgCl). Note that in terms of electrochemistry, the sign of the corresponding electrochemical potential (E) and Faradaic current (i) of MR-1 is opposite to the applied V_G and measured I_G, as the source electrode (working electrode) is set at ground. (e) In device CV of MR-1. (f) I_g–V_g (CV, black curve) and corresponding I_{sd}–V_g (ETS, green curve) characteristics of a typical MR-1 device.

relatively small current signals. The details of device fabrication and measurement setup are described in the Methods section.

The measurement of *S. oneidensis* MR-1 was conducted under both aerobic and anaerobic conditions. Typically, the MR-1 cell culture was injected into the PDMS chamber after a stable baseline was established in media solution. The source–drain current (I_{sd}) was continuously recorded at the rate of 2 Hz with a constant bias voltage (V_{sd}) of 50 mV. The current–time (I–t) characteristics of *S. oneidensis* MR-1 in aerobic and anaerobic conditions are shown in Figure 1c. As expected, increased I_{sd} over time was observed under both conditions after introduction of the MR-1 culture. The I–t characteristics of MR-1 were slightly different in these two different environments. In anaerobic measurements, a jump in current was observed immediately, followed by a faster increase. For measurements under aerobic conditions, the current remained negligible (*i.e.*, the same as that in media background) for *ca.* 40 to 60 min before it started to increase gradually (note that the sharp current "spike" just after the injection of the MR-1 culture is not correlated to the MR-1, but is due to the disturbance and reformation of the electrical double layer on the electrodes). The delayed current increase is likely due to the presence of dissolved oxygen. Assuming I_{sd} is correlated to the EET process of MR-1, either oxygen acts as an electron acceptor in the EET process, or in the presence of oxygen, EET is not involved in MR-1 metabolism. When oxygen is consumed near the electrode surface, a local anaerobic environment is established for the subsequent electron transfer to electrode and thus current generation. For both conditions, the current reached steady state after about 2 h of MR-1 exposure, indicating a similar (locally anaerobic) condition of MR-1 cells attached onto the electrodes. This result is further confirmed by the similar current–voltage (I–V) characteristics of MR-1 measured at steady state under both aerobic and anaerobic conditions (Figure 1e). By "steady state" we mean here that the currents have become stable and do not vary with time. These I_{sd}–V_{sd} characteristics offer valuable insights into the charge transport dynamics of actively respiring *S. oneidensis* MR-1. After the I_{sd} current was observed, an injection of 0.25% glutaraldehyde as a biocide[26] completely quenched the current (Figure 1d), verifying that the conducting current measured in this system originates from living MR-1 cell(s). Furthermore, *in situ* dark-field optical imaging during the electrical measurements was performed, MR-1 was observed to swim to the chip surface and was immobilized gradually on the electrode (some also landed and stayed between the source and drain electrodes, as shown in Figure 1f). This result confirmed that the observed I_{sd} is correlated with the attachment of MR-1 cells onto the electrodes. The scanning electron microscope (SEM) images of the device after the measurements (Figure 1g) show individual MR-1 cells attached onto the electrodes and bridging the gap. Bacterial nanowires were not observed during the measurements, as determined by both *in situ* optical microscopy and *ex situ* SEM characterization (Figure 1f,g). Our results indicate that apparent charge transport is observed in MR-1 cells even without conductive bacterial nanowires.[16,17] When the device was exposed to MR-1 for a longer period of time (12 to 24 h), the I_{sd} further increased to another plateau, and *ex situ* SEM measurements confirmed the formation of a thin biofilm layer (with a typical thickness between 1 to 3 μm). Similar I–V characteristics with larger amplitude (as compared to the 2 h sample) were observed for the *Shewanella* biofilm (see Supporting Information Figure S1).

DOI: 10.1021/acsnano.6b03655
ACS Nano 2016, 10, 9919–9926

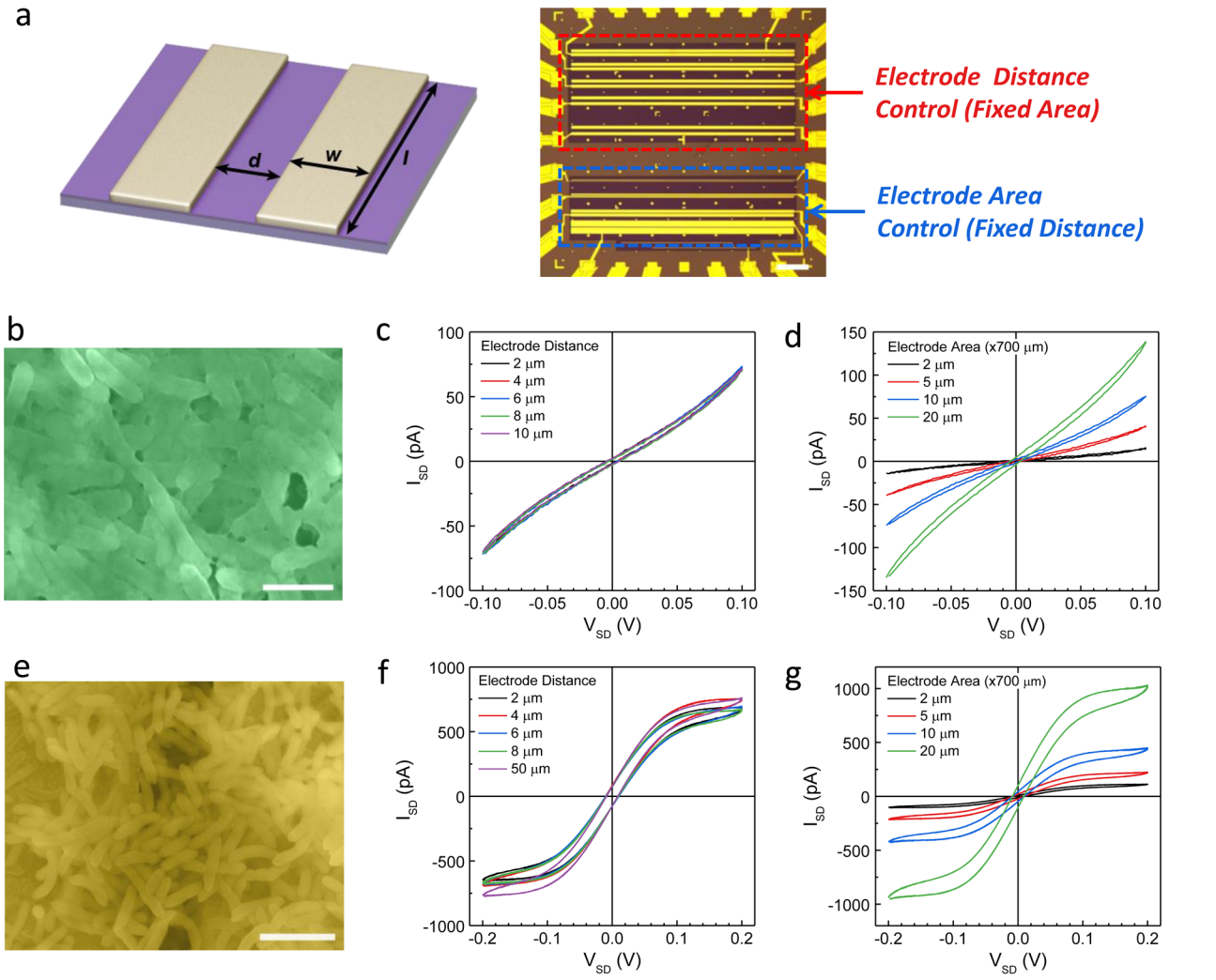

Figure 3. Nanoelectronic investigation of the "electrical conduction" of *Shewanella* and *Geobacter* biofilms using electrode pairs with varying gaps and areas. (a) Schematic illustration of the biofilm measurements using two sets of pair electrodes with either varying gaps (with fixed areas) or varying electrode areas (with fixed gaps). (b) Representative SEM image of a *Shewanella* biofilm. (c, d) I_{sd}–V_{sd} behavior of living *Shewanella* biofilms with different pair electrode distances (c) and different electrode areas (d). (e) Representative SEM image of a *Geobacter* biofilm grown under anaerobic conditions. (f, g) I_{sd}–V_{sd} behavior of living *Geobacter* biofilms with different electrode distances (f) and different electrode areas (g). Scale bars in (b) and (e) are 2 μm.

The above electrical transport measurements show apparent electrical conductivity in *S. oneidensis* MR-1 similar to previous studies in electrogenic microbial systems.[16,17,20−22] To gain further mechanistic insight and to elucidate the origins of such electrical conductivity, we used electrical transport spectroscopy (ETS)[27] to probe the microbial system under physiological conditions. The ETS approach introduces an additional reference electrode (RE) and a counter electrode (CE) into the nanoelectronic on-chip measurement platform (Figure 2a). Analogous to a conventional field-effect transistor (FET), the counter electrode functions as a gate electrode, and the reference electrode (Ag/AgCl) is used to establish the electrochemical potentials of MR-1. This platform enables concurrent measurements of the gate current (I_g) and the electrical transport current (I_{sd}) in microbial samples (see Methods).

Our measurements show that the electrical transport current (I_{sd}) (blue line in Figure 2b) and gate current (I_g) (red line in Figure 2b) exhibit comparable amplitudes, but with opposite polarities. While I_{sd} is considered the electrical transport current, I_g is generally recognized as "leakage current" in a typical FET measurement. Such leakage currents are undesirable for both solid-state FETs and electrolyte-gated FETs, as the electrical transport (I_{sd}) is expected to be altered only by the electrical field across a dielectric layer for a solid-state FET, or an electrolyte double layer for an electrolyte-gated FET; negligible current should be observed through the gating channel. The considerable I_g observed in MR-1 can be attributed to the Faradaic current (*i.e.*, redox current) originating from electron transfer at the cell/electrode interface.[27] This conclusion is also supported by the negligible I_g observed in the free medium control (see Supporting Information Figure S4). The comparable I_g and I_{sd} from living MR-1 indicate that electrochemical current (I_g) contributes at least partly to the electrical transport current (I_{sd}). With an I_g of comparable amplitude, the measured I_{sd} is convoluted with I_g. We have previously shown in our ETS studies that the contributions of I_g to I_{sd} can be properly deducted by considering the equivalent circuit (see Supporting Information Figure S5) to obtain I_{sd} accurately (green curve in Figure 2b).[27]

DOI: 10.1021/acsnano.6b03655
ACS Nano 2016, 10, 9919−9926

Together, our results provide the first example of direct and concurrent measurements of the electrochemical (I_g) and electrical transport (I_{sd}) currents of *S. oneidensis* MR-1 under physiological conditions, enabling a more comprehensive and conclusive analysis of the system.

The above discussions indicate that electron transport within MR-1 is closely correlated to electrochemical processes. More detailed analyses of the results further support this hypothesis. When the gate voltage is set negative (*vs* a Ag/AgCl reference), the actual electrochemical potentials of MR-1 are more oxidizing, leading to enhanced digestion (oxidation) of electron donors and and increase in I_g (absolute value) (Figure 2c respiration "on" state). With a positive gate voltage (*vs* Ag/AgCl), MR-1 cells are pinned at a more reducing electrochemical potential. This situation suppresses metabolic oxidation and significantly reduces I_g (Figure 2c, respiration "off" state).

The $I_{sd}-V_{sd}$ characteristics show similar trends to that of I_g (Figure 2d). Specifically, when MR-1 is pinned at an oxidative potential, the device shows considerably increased I_{sd} (larger slope in $I_{sd}-V_{sd}$ curve), demonstrating that the electrical transport current depends strongly on the electrochemical states of MR-1. Hence, a small change in V_{sd} can produce a large modulation in I_{sd} and a large $I_{sd}-V_{sd}$ slope. In contrast, when the MR-1 is set at a reductive potential and respiration–off state, the modulation of I_{sd} by V_{sd} is much smaller, and thus the $I_{sd}-V_{sd}$ slope is smaller (Figure 2d). Given that V_{sd} actually modulates the electrochemical potentials (V_g), this behavior is consistent with our hypothesis that the overall electron conductive current (I_{sd}) originates at least partially from the electrochemical current. Another approach for ETS investigation is to perform on-chip cyclic voltammetry (CV) of MR-1 while monitoring the corresponding change of their conductivity (by measuring I_{sd} at a constant V_{sd}). As shown in Figure 2e,f, typical CV characteristics of MR-1 in electron-donor-rich media were observed on-chip (Figure 2e), but unlike a conducting material system that has distinguishable ETS (I_{sd}-V_g) characteristics in response to the electrochemical processes,[27] MR-1 shows an ETS current (I_{sd}) that is inversely proportional to the corresponding CV current (I_g), which provides additional evidence for the electrochemical origins of the conducting current measured from MR-1.

Note that electrochemically generated current has not been previously considered responsible for the electrical transport current observed in such microbial systems. A major reason is that it is relatively difficult to separate out the electrochemical current, especially under physiological conditions. Our on-chip ETS approach enables separate and concurrent measurement of Faradaic current and electrical transport current from living MR-1 and is thus well suited for such investigations.

To test our hypothesis more conclusively and quantitatively, inspired by the ETS measurements of actively respiring MR-1, we investigated the dependence of electrical conduction ($I_{sd}-V_{sd}$) on the electrode gap distance and the area of the electrodes. These parameters provide key insight into the conduction mechanism in typical nanoelectronic studies. In metal- or semiconductor-based conductive pathways (as suggested in recent debates on the studies of *Geobacter*),[18−24] the measured currents should be inversely proportional to the distance between the conducting channels and be independent of the electrode area, whereas electrochemically related currents are expected to have the opposite correlation, *i.e.*, to be proportional to the electrode area and independent of electrode distance. Therefore, the $I_{sd}-V_{sd}$ dependence on the pair electrode distance and area can be used to probe the role of electrochemical current directly in the electron conduction measurement and to elucidate unambiguously the quantitative contribution from the electrochemical current to the overall electrical transport current. To this end, we have designed electrode arrays with varying electrode areas and electrode distances (Figure 3a) and conducted systematic electrical transport studies. Surprisingly, I_{sd} from MR-1 (either individual cells or biofilms) exhibits no dependence on the pair electrode distance but shows strong correlation with the electrode area (Figure 3c,d and Supporting Information Figure S6). This observation offers direct evidence that the electrical conduction current (I_{sd}) from MR-1 largely originates from the electrochemical current that is generated at the cell/electrode interface.

Due to the paucity of documented electrical measurements of living *Shewanella* for reference, we have conducted analogous investigations on biofilms of *Geobacter sulfurreducens* PCA (Figure 3e). Therefore, previously reported results/models on the *G. sulfurreducens* can be used to cross-reference the data and the conclusions obtained in this study. Similarly, the PCA biofilms were grown *in situ* on the device by a previously developed anode growth method[20,21] and studied under physiological conditions using the same approach described above. The $I_{sd}-V_{sd}$ measurement of *Geobacter* biofilms also shows that current is not dependent on the electrode distance but is only related to electrode area (Figure 3f,g), indicating the same interfacial electrochemistry model that we proposed for *Shewanella*. These results argue against the previously suggested superexchange model and metal/semiconductor model in which the current should be inversely proportional to the distance between the two electrodes. Also, note that the $I-V$ characteristics observed for the *Geobacter* biofilms show sigmoidal shapes (distinct from that of *Shewanella*) with steady-state currents at high voltages. Although the superexchange hypothesis where the current is driven by a redox gradient (first developed to describe the charge transport in electroactive polymers with fixed molecular redox sites)[28,29] can also be used to explain the sigmoidal $I-V$ characteristics of *Geobacter* biofilms,[21,22,24] it does not explain the different $I-V$ characteristics observed for *Shewanella* or the lack of distance dependence of the *Geobacter*'s $I-V$ behavior.

The lack of distance dependence and the distinct area dependence of the measured current strongly suggest that the electrical conduction from *Shewanella* and *Geobacter* are dominated by the electrochemical current generated at the cell/electrode interfaces. The transport current across the source and drain electrodes is attributed to the different electrochemical current (turnover rate) at the source and drain electrodes due to slightly different potentials (resulted from the V_{sd} bias), which leads to an ionic current across the source–drain electrodes to balance the charge. As similar nanoelectronic fabrication techniques and investigations have not previously been employed for microbial studies, our study suggests that this approach can elucidate important factors and insights that were missed previously. In particular, the area of electrodes exposed to the living bacteria/biofilm and/or medium environment should be carefully controlled in such investigations, and the current dependence on the electrode distance should be investigated for proposed transport mechanisms.

DOI: 10.1021/acsnano.6b03655
ACS Nano 2016, 10, 9919–9926

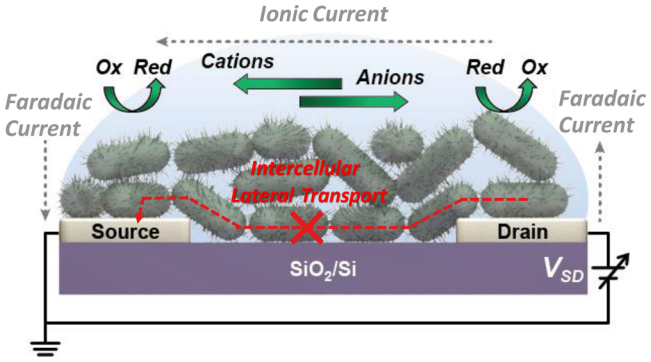

Figure 4. Schematic illustration of the interface electrochemistry model for the electrical conducting current in a typical electrode pair measurement. The transport current is determined by the vertical electron transfer (electrochemical/Faradaic current) at the bacteria/electrode interfaces, whereas lateral (non-Faradaic) electron transport pathway across the biofilm does not exist. Ionic transport (current) toward the electrodes in the lateral direction forms a complete electrochemical circuit.

Figure 4 schematically illustrates the interface electrochemistry model. The transport current across the source–drain electrodes is limited by Faradaic electron transfer at the bacteria/electrode interface (electrochemical current) and is coupled with ionic transport current in the lateral direction to form a complete electrochemical circuit. On the other hand, the previously suggested electron transport pathway across the biofilm, either by electron hopping through a network of redox centers or *via* the intrinsic metallic-like conductivity, does not exist or does not play a significant role in the system we are studying here. Additional results that are consistent with our conclusions are the observation of I_{sd}–V_{sd} current in the case where cellular bridges have not formed to connect the pair electrodes physically (Supporting Information Figure S6). Once the origins of the conducting current from these microbiomes are clarified, their measurement can be used to elucidate the mechanism of the corresponding EET process. For instance, with the interface electrochemistry model, the long-range electron transport across the electrically conductive biofilm thickness (through either the metallic pili mechanism or the redox matrix mechanism) has been called into question. Therefore, this model weighs in favor of two redox-based EET mechanisms: direct contact (*via* membrane cytochromes) or "electron shuttling" (*via* secreted mediators).

It has been previously suggested that *Shewanella* and *Geobacter* undergo different EET pathways. For *Shewanella*, extracellular electrons are transferred to the electrode *via* cell-secreted flavins that diffuse to the electrode surface and act as redox mediators (*i.e.*, the indirect "electron shuttling" mechanism);[25,30–32] for *Geobacter*, on the other hand, electrons are directly transferred to the electrode through outer membrane c-type cytochrome (c-Cyts) protein that is in physical contact with the electrode surface (direct contact mechanism).[33,34] Interestingly, the distinct conductive *I*–*V* characteristics observed for *Shewanella* and *Geobacter* in this study can be rationalized with the different EET mechanisms in these two model bacteria. Specifically, the sigmoidal *I*–*V* characteristic (Figure 3f) obtained from *Geobacter* can be explained by the combination of the direct electron transfer mechanism and our interfacial electrochemistry model. With relatively efficient electron transfer kinetics at the cytochrome/electrode interface, the overall electron transfer rate and, therefore, the Faradaic current at relatively high bias are limited by the catalytic rate of the enzyme/electrode system or the diffusion-limited supply of the redox species,[35,36] thus leading to a steady-state current that is independent of the bias voltage at relatively higher potentials and sigmoidal *I*–*V* behavior of *Geobacter* (following the Nernst–Monod equation).[35,36] As for *Shewanella*, the current generation is limited by the relatively slow kinetics of the interface electron transfer (*i.e.*, redox of flavin on the electrode), and thus its *I*–*V* behavior follows the Butler–Volmer equation[35,36] and increases with bias voltage without apparent saturation in the measurement range. Therefore, our interface electrochemistry model for the mechanism of microbial electrical conductivity, along with corresponding experimental observations, provide additional evidence and important insight into the EET mechanisms of both *Shewanella* and *Geobacter* systems and might also shed light on the fundamental basis of electron transport in other microbial systems.[37] Future investigations of genetically engineered microbial systems (*e.g.*, *Shewanella* strains lacking specific functional proteins *via* selective gene deletion) could offer further insight into the charge transport mechanisms in these microbial systems.

CONCLUSIONS AND PROSPECTS

We have employed nanoelectronic fabrication and measurements to elucidate the origins of the electrical conducting current from two model electrogenic microbial systems, *S. oneidensis* MR-1 and *G. sulfurreducens* PCA. The electrical characteristics of each strain were obtained under physiological conditions together with *in situ* optical imaging and other on-chip measurements. We have shown that the conductive current from these microbes originates from electrochemical electron transfer at the cell/electrode interface, and no lateral electron transport across the cell or biofilm was observed. The experimental data reported in this study indicate that results and the interpretations made in earlier experimental and theoretical studies should be revisited, particularly paying attention to electrode distance/area dependence (which has not always been measured or reported). Furthermore, our interface electrochemistry model provides valuable insight into the EET mechanisms of both model microbial systems. From a broader perspective, these nanoelectronic testbeds and investigations reveal important factors and insights into microbial studies. These tools will accelerate our basic understanding of earth's microbiomes and harness the capabilities of microbial ecosystems.[38–41]

METHODS

Growth of *Shewanella oneidensis* MR-1 and *Geobacter sulfurreducens* PCA. *S. oneidensis* strain MR-1 was grown aerobically in LB broth (20 g/L, 20 mL, Sigma-Aldrich) with gentle shaking (200 rpm) at 30 °C for approximately 12 h. The cells were then redispersed into fresh LB broth at a volume ratio of 1:100. The redispersed culture was shaken (200 rpm) aerobically for approximately 6 h at 30 °C (up to an OD_{600} of 0.5) before measurements. *G. sulfurreducens* strain PCA was grown in a continuous flow bioreactor (BioFlo 110; New Brunswick Scientific) with a medium inflow rate of 0.4 mL/min and a working volume of 1 L. Sodium acetate (20 mM) was used as electron donor and sodium fumarate (480 mM) as electron acceptor. In addition, the growth medium contained the following chemicals as nutrients (in mg/L): NH_4Cl, 200; $NaH_2PO_4 \cdot H_2O$, 69; KCl, 380; $CaCl_2 \cdot H_2O$, 40; $MgSO_4 \cdot 7H_2O$, 200, nitrilotriacetic acid, 15; $MnCl \cdot 4H_2O$, 10; $FeSO_4 \cdot 7H_2O$, 5; $CoCl_2 \cdot 6H_2O$, 2; $ZnCl_2$, 1; $CuSO_4 \cdot 5H_2O$, 0.3; $AlK(SO_4)_2 \cdot 12H_2O$, 0.05; H_3BO_3, 0.05; Na_2MoO_4,

DOI: 10.1021/acsnano.6b03655
ACS Nano 2016, 10, 9919–9926

0.9; $NiCl_2$, 0.5; $Na_2WO_4{\cdot}2H_2O$, 0.2; Na_2SeO_4, 1. The culture media were maintained at 25 °C and at pH = 7. A mixture of N_2:CO_2 (80:20) was constantly flowing into the reactor (0.4 mL/min) to remove any traces of oxygen and to maintain a strictly anaerobic environment. The culture in the reactor was stirred at a constant speed of 50 rpm. The PCA cell culture in the flow reactor was kept at a steady state with a measured OD_{600} of 0.6 before measurements.

Fabrication of the Pair Electrode Device. Pair electrodes (as source and drain) on the substrate (p^{+2} silicon wafer with 300 nm thermal oxide) were defined by EBL, followed by evaporation of 20 nm Ti and 50 nm Au. To eliminate the influence of electrolyte and to avoid electrochemical reactions on the metal electrodes, a passivation layer of poly(methyl methacrylate) (PMMA, ~500 nm thick, electrochemically inert) was spin-coated on the device. Windows that only exposed desired areas and electrodes to the samples were opened by EBL.

Electrical Measurement and *in Situ* Optical Imaging of Living Cells. A source measurement unit (SMU, Agilent B2902a) was used for all microbial measurements. For $I-t$ measurements, source−drain current was recorded at a rate of 2 Hz, with a small bias voltage of 50 mV. Typically, the MR-1 cell culture was injected into the PDMS chamber after a stable baseline was established in medium solution. For $I-V$ measurements, the source−drain voltage was swept between −0.1 and 0.1 V at a typical rate of 10 mV/s to minimize the capacitive charging current (appeared as hysteresis in $I-V$ curve). All anaerobic measurements were carried out in an anaerobic hood (Coy Anaerobic Chamber, Type B, Vinyl) with an in-hood probe station. *In situ* optical imaging was carried out with an upright microscope (QImaging Retiga 2000R) operated under dark-field.

Gating and ETS Measurement. The two-channel SMU was used for the gate measurement (one as a gate channel and one as a source−drain channel). A four-probe configuration was used with a gate channel to function as a potentiostat.[27] The potential of the drain electrode was controlled with respect to the reference electrode (V_g *vs* Ag/AgCl), while the current (I_g) was collected and measured through the counter electrode. The source−drain channel was used either to supply a small bias potential (50 mV) between source and drain electrodes and collect the corresponding current (I_{sd}) during a V_g sweep or to sweep the source−drain voltage (V_{sd}) at an applied gate voltage (V_g) to obtain the $I_{sd}-V_{sd}$ curve. The equivalent circuit of the ETS measurement is illustrated in Supporting Information Figure S5.

ASSOCIATED CONTENT

Supporting Information

The Supporting Information is available free of charge on the ACS Publications website at DOI: 10.1021/acsnano.6b03655.

Additional $I-t$, $I-V_g$, and $I-V$ measurements (PDF)

AUTHOR INFORMATION

Corresponding Authors

*E-mail: xduan@chem.ucla.edu.
*E-mail: yhuang@seas.ucla.edu.

Author Contributions

○These authors contributed equally. M.D., H.-Y.S., G.W., P.S.W., G.C.L.W., K.H.N., Y.H., and X.D. designed the research; M.D. conducted the electrical measurement with the assistance of H.-Y.S.; H.-Y.S. and S.-H.L. prepared the microbial cultures with the assistance of C.K.L., M.D., G.W., and T.D.Y.; M.D. and X.D. analyzed the data and wrote the paper with the assistance of all the authors; P.S.W., G.C.L.W., K.H.N., Y.H., and X.D. supervised the research.

Notes

The authors declare no competing financial interest.

ACKNOWLEDGMENTS

We gratefully acknowledge the support of the Office of Naval Research grant N000141410051. We thank Dr. Linda Chrisey for suggesting control experiments and critique of earlier versions of this paper.

REFERENCES

(1) Nealson, K. H.; Saffarini, D. Iron and Manganese in Anaerobic Respiration: Environmental Significance, Physiology, and Regulation. *Annu. Rev. Microbiol.* **1994**, *48*, 311−343.
(2) Fredrickson, J. K.; Romine, M. F.; Beliaev, A. S.; Auchtung, J. M.; Driscoll, M. E.; Gardner, T. S.; Nealson, K. H.; Osterman, A. L.; Pinchuk, G.; Reed, J. L.; Rodionov, D. A.; Rodrigues, J. L. M.; Saffarini, D. A.; Serres, M. H.; Spormann, A. M.; Zhulin, I. B.; Tiedje, J. M. Towards Environmental Systems Biology of *Shewanella*. *Nat. Rev. Microbiol.* **2008**, *6*, 592−603.
(3) Logan, B. E.; Rabaey, K. Conversion of Wastes Into Bioelectricity and Chemicals by Using Microbial Electrochemical Technologies. *Science* **2012**, *337*, 686−690.
(4) Hau, H. H.; Gralnick, J. A. Ecology and Biotechnology of the Genus *Shewanella*. *Annu. Rev. Microbiol.* **2007**, *61*, 237−258.
(5) Rabaey, K.; Rozendal, R. A. Microbial Electrosynthesis - Revisiting the Electrical Route for Microbial Production. *Nat. Rev. Microbiol.* **2010**, *8*, 706−716.
(6) Sakimoto, K. K.; Wong, A. B.; Yang, P. Self-Photosensitization of Nonphotosynthetic Bacteria for Solar-to-Chemical Production. *Science* **2016**, *351*, 74−77.
(7) Lovley, D. R. Bug Juice: Harvesting Electricity with Microorganisms. *Nat. Rev. Microbiol.* **2006**, *4*, 497−508.
(8) Logan, B. E. Exoelectrogenic Bacteria That Power Microbial Fuel Cells. *Nat. Rev. Microbiol.* **2009**, *7*, 375−381.
(9) Lovley, D. R. Electromicrobiology. *Annu. Rev. Microbiol.* **2012**, *66*, 391−409.
(10) Schroder, U.; Harnisch, F.; Angenent, L. T. Microbial Electrochemistry and Technology: Terminology and Classification. *Energy Environ. Sci.* **2015**, *8*, 513−519.
(11) Rabaey, K.; Verstraete, W. Microbial Fuel Cells: Novel Biotechnology for Energy Generation. *Trends Biotechnol.* **2005**, *23*, 291−298.
(12) Du, Z.; Li, H.; Gu, T. A State of the Art Review on Microbial Fuel Cells: A Promising Technology for Wastewater Treatment and Bioenergy. *Biotechnol. Adv.* **2007**, *25*, 464−482.
(13) Borole, A. P.; Reguera, G.; Ringeisen, B.; Wang, Z.-W.; Feng, Y.; Kim, B. H. Electroactive Biofilms: Current Status and Future Research Needs. *Energy Environ. Sci.* **2011**, *4*, 4813−4834.
(14) Yang, Y.; Xu, M.; Guo, J.; Sun, G. Bacterial Extracellular Electron Transfer in Bioelectrochemical Systems. *Process Biochem.* **2012**, *47*, 1707−1714.
(15) Okamoto, A.; Nakamura, R.; Nealson, K. H.; Hashimoto, K. Bound Flavin Model Suggests Similar Electron-Transfer Mechanisms in *Shewanella* and *Geobacter*. *ChemElectroChem* **2014**, *1*, 1808−1812.
(16) Gorby, Y. A.; Yanina, S.; McLean, J. S.; Rosso, K. M.; Moyles, D.; Dohnalkova, A.; Beveridge, T. J.; Chang, I. S.; Kim, B. H.; Kim, K. S.; Culley, D. E.; Reed, S. B.; Romine, M. F.; Saffarini, D. A.; Hill, E. A.; Shi, L.; Elias, D. A.; Kennedy, D. W.; Pinchuk, G.; Watanabe, K.; et al. Electrically Conductive Bacterial Nanowires Produced by *Shewanella oneidensis* Strain MR-1 and Other Microorganisms. *Proc. Natl. Acad. Sci. U. S. A.* **2006**, *103*, 11358−11363.
(17) Leung, K. M.; Wanger, G.; El-Naggar, M. Y.; Gorby, Y.; Southam, G.; Lau, W. M.; Yang, J. *Shewanella oneidensis* MR-1 Bacterial Nanowires Exhibit *p*-Type, Tunable Electronic Behavior. *Nano Lett.* **2013**, *13*, 2407−2411.
(18) Malvankar, N. S.; Tuominen, M. T.; Lovley, D. R. Comment on "On Electrical Conductivity of Microbial Nanowires and Biofilms". *Energy Environ. Sci.* **2012**, *5*, 6247−6249.
(19) Malvankar, N. S.; Tuominen, M. T.; Lovley, D. R. Lack of Cytochrome Involvement in Long-Range Electron Transport through

DOI: 10.1021/acsnano.6b03655
ACS Nano 2016, 10, 9919−9926

Conductive Biofilms and Nanowires of *Geobacter sulfurreducens*. *Energy Environ. Sci.* **2012**, *5*, 8651−8659.
(20) Malvankar, N. S.; Vargas, M.; Nevin, K. P.; Franks, A. E.; Leang, C.; Kim, B.-C.; Inoue, K.; Mester, T.; Covalla, S. F.; Johnson, J. P.; Rotello, V. M.; Tuominen, M. T.; Lovley, D. R. Tunable Metallic-Like Conductivity in Microbial Nanowire Networks. *Nat. Nanotechnol.* **2011**, *6*, 573−579.
(21) Snider, R. M.; Strycharz-Glaven, S. M.; Tsoi, S. D.; Erickson, J. S.; Tender, L. M. Long-Range Electron Transport in *Geobacter sulfurreducens* Biofilms is Redox Gradient-Driven. *Proc. Natl. Acad. Sci. U. S. A.* **2012**, *109*, 15467−15472.
(22) Strycharz-Glaven, S. M.; Snider, R. M.; Guiseppi-Elie, A.; Tender, L. M. On the Electrical Conductivity of Microbial Nanowires and Biofilms. *Energy Environ. Sci.* **2011**, *4*, 4366−4379.
(23) Strycharz-Glaven, S. M.; Tender, L. M. Reply to the 'Comment on "On Electrical Conductivity of Microbial Nanowires and Biofilms"'. *Energy Environ. Sci.* **2012**, *5*, 6250−6255.
(24) Yates, M. D.; Golden, J. P.; Roy, J.; Strycharz-Glaven, S. M.; Tsoi, S.; Erickson, J. S.; El-Naggar, M. Y.; Calabrese Barton, S.; Tender, L. M. Thermally Activated Long Range Electron Transport in Living Biofilms. *Phys. Chem. Chem. Phys.* **2015**, *17*, 32564−32570.
(25) Jiang, X.; Hu, J.; Fitzgerald, L. A.; Biffinger, J. C.; Xie, P.; Ringeisen, B. R.; Lieber, C. M. Probing Electron Transfer Mechanisms in *Shewanella oneidensis* MR-1 Using a Nanoelectrode Platform and Single-Cell Imaging. *Proc. Natl. Acad. Sci. U. S. A.* **2010**, *107*, 16806−16810.
(26) Jiang, X.; Hu, J.; Petersen, E. R.; Fitzgerald, L. A.; Jackan, C. S.; Lieber, A. M.; Ringeisen, B. R.; Lieber, C. M.; Biffinger, J. C. Probing Single- to Multi-Cell Level Charge Transport in *Geobacter sulfurreducens* DL-1. *Nat. Commun.* **2013**, *4*, 2751.
(27) Ding, M.; He, Q.; Wang, G.; Cheng, H.-C.; Huang, Y.; Duan, X. An On-Chip Electrical Transport Spectroscopy Approach for *in Situ* Monitoring Electrochemical Interfaces. *Nat. Commun.* **2015**, *6*, 7867.
(28) Pickup, P. G.; Murray, R. W. Redox Conduction in Mixed-Valent Polymers. *J. Am. Chem. Soc.* **1983**, *105*, 4510−4514.
(29) Dalton, E. F.; Surridge, N. A.; Jernigan, J. C.; Wilbourn, K. O.; Facci, J. S.; Murray, R. W. Charge Transport in Electroactive Polymers Consisting of Fixed Molecular Redox Sites. *Chem. Phys.* **1990**, *141*, 143−157.
(30) Marsili, E.; Baron, D. B.; Shikhare, I. D.; Coursolle, D.; Gralnick, J. A.; Bond, D. R. *Shewanella* Secretes Flavins That Mediate Extracellular Electron Transfer. *Proc. Natl. Acad. Sci. U. S. A.* **2008**, *105*, 3968−3973.
(31) Newman, D. K.; Kolter, R. A Role for Excreted Quinones in Extracellular Electron Transfer. *Nature* **2000**, *405*, 94−97.
(32) Brutinel, E. D.; Gralnick, J. A. Shuttling Happens: Soluble Flavin Mediators of Extracellular Electron Transfer in *Shewanella*. *Appl. Microbiol. Biotechnol.* **2012**, *93*, 41−48.
(33) Bond, D. R.; Lovley, D. R. Electricity Production by *Geobacter sulfurreducens* Attached to Electrodes. *Appl. Environ. Microbiol.* **2003**, *69*, 1548−1555.
(34) Reguera, G.; Nevin, K. P.; Nicoll, J. S.; Covalla, S. F.; Woodard, T. L.; Lovley, D. R. Biofilm and Nanowire Production Leads to Increased Current in *Geobacter sulfurreducens* Fuel Cells. *Appl. Environ. Microbiol.* **2006**, *72*, 7345−7348.
(35) Torres, C. I.; Marcus, A. K.; Lee, H.-S.; Parameswaran, P.; Krajmalnik-Brown, R.; Rittmann, B. E. A Kinetic Perspective on Extracellular Electron Transfer by Anode-Respiring Bacteria. *FEMS Microbiol. Rev.* **2010**, *34*, 3−17.
(36) Léger, C.; Bertrand, P. Direct Electrochemistry of Redox Enzymes as a Tool for Mechanistic Studies. *Chem. Rev.* **2008**, *108*, 2379−2438.
(37) Pfeffer, C.; Larsen, S.; Song, J.; Dong, M.; Besenbacher, F.; Meyer, R. L.; Kjeldsen, K. U.; Schreiber, L.; Gorby, Y. A.; El-Naggar, M. Y.; Leung, K. M.; Schramm, A.; Risgaard-Petersen, N.; Nielsen, L. P. Filamentous Bacteria Transport Electrons Over Centimetre Distances. *Nature* **2012**, *491*, 218−221.
(38) Alivisatos, A. P.; Blaser, M. J.; Brodie, E. L.; Chun, M.; Dangl, J. L.; Donohue, T. J.; Dorrestein, P. C.; Gilbert, J. A.; Green, J. L.; Jansson, J. K.; Knight, R.; Maxon, M. E.; McFall-Ngai, M. J.; Miller, J. F.; Pollard, K. S.; Ruby, E. G.; Taha, S. A. A Unified Initiative to Harness Earth's Microbiomes. *Science* **2015**, *350*, 507−508.
(39) Stulberg, E.; Fravel, D.; Proctor, L. M.; Murray, D. M.; LoTempio, J.; Chrisey, L.; Garland, J.; Goodwin, K.; Graber, J.; Harris, M. C.; Jackson, S.; Mishkind, M.; Porterfield, D. M.; Records, A. An Assessment of US Microbiome Research. *Nat. Microbiol.* **2016**, *1*, 15015.
(40) Biteen, J. S.; Blainey, P. C.; Cardon, Z. G.; Chun, M.; Church, G. M.; Dorrestein, P. C.; Fraser, S. E.; Gilbert, J. A.; Jansson, J. K.; Knight, R.; Miller, J. F.; Ozcan, A.; Prather, K. A.; Quake, S. R.; Ruby, E. G.; Silver, P. A.; Taha, S.; van den Engh, G.; Weiss, P. S.; Wong, G. C. L.; et al. Tools for the Microbiome: Nano and Beyond. *ACS Nano* **2016**, *10*, 6−37.
(41) Lee, C. K.; Kim, A. J.; Santos, G. S.; Lai, P. Y.; Lee, S. Y.; Qiao, D. F.; De Anda, J.; Young, T. D.; Chen, Y.; Rowe, A. R.; Weiss, P. S.; Nealson, K. H.; Wong, G. C. L. Evolution of Cell Size Homeostasis and Growth Rate Diversity during Initial Surface Colonization of *Shewanella oneidensis*. *ACS Nano* **2016**, *10*, 9183−9192.

DOI: 10.1021/acsnano.6b03655
ACS Nano 2016, 10, 9919−9926